optica

Sub-100-fs 1.87 GHz mode-locked fiber laser using stretched-soliton effects

W. He,[1] M. Pang,[1,*] C. R. Menyuk,[1,2] and P. St. J. Russell[1]

[1]Max Planck Institute for the Science of Light, Staudtstrasse 2, 91058 Erlangen, Germany
[2]Department of Computer Science and Electrical Engineering, University of Maryland Baltimore County, Baltimore, Maryland 21250, USA
*Corresponding author: meng.pang@mpl.mpg.de

Received 6 September 2016; revised 24 October 2016; accepted 24 October 2016 (Doc. ID 275219); published 14 November 2016

Current pulsed fiber lasers that are capable of delivering stable sub-100-fs pulses at megahertz repetition rates require intracavity pulse energies in the nanojoule range. Scaling these lasers to gigahertz repetition rates necessitates, therefore, very high average power levels and complex cladding-pumped configurations. Here we report a type of stretched-soliton all-fiber laser that generates broadband, soliton-like pulses at 1.55 μm with intracavity pulse energies of only tens of picojoules. In the laser cavity, strong dispersion management leads to a temporal breathing ratio of ~70, while the weak residual anomalous dispersion is perfectly balanced by the low Kerr nonlinearity, resulting in the formation of temporally stretched, hyperbolic-secant pulses. A lumped wavelength-dependent attenuator compensates for the effects of the gain filtering on the pulse spectrum, ensuring intracavity pulse self-consistency. This unique stretched-soliton mechanism, combined with a harmonic mode-locking technique based on intense optoacoustic interactions in solid-core photonic crystal fiber, yields for the first time stable gigahertz-rate, sub-100-fs, dispersive-wave-free pulse trains at moderate pump powers.

OCIS codes: (140.7090) Ultrafast lasers; (060.5295) Photonic crystal fibers; (140.3510) Lasers, fiber.

http://dx.doi.org/10.1364/OPTICA.3.001366

1. INTRODUCTION

Fiber lasers offering gigahertz repetition rates and ultrashort pulse durations have many potential applications in frequency metrology, arbitrary waveform generation, optical telecommunications, biomedicine, femtochemistry and material processing [1–5]. The practical advantages of all-fiber laser configurations—compactness, efficient heat dissipation, high beam quality, and easy alignment—make them highly sought-after. The first all-fiber mode-locked laser used Er-doped fiber (EDF) as a gain medium, with an operating wavelength of 1550 nm [6,7]. Since standard single-mode fiber (SMF) has strong anomalous dispersion in this wavelength region, early mode-locked EDF lasers generated optical solitons with durations from several hundred femtoseconds to several picoseconds [8–10]. Pulse shortening in soliton fiber lasers is, however, restricted by the fundamental properties of solitons [11]. According to the soliton area theorem [12], a higher energy is necessary for a shorter pulse duration, which further increases the pulse peak power, leading to large accumulated nonlinear phase shift and thus sideband instabilities in soliton lasers [13,14]. To eliminate these restrictions on pulse duration, stretched-pulse operation of a fiber laser was introduced by Tamura *et al.* [15]. In stretched-pulse fiber lasers, the use of alternating fiber sections of normal and anomalous dispersion leads to both temporal and spectral breathing of the pulses. While the temporal breathing significantly reduces the accumulated nonlinear phase shift of laser pulses over a single cavity round trip [16–18], the cooperation of pulse chirp and Kerr nonlinearity leads to spectral breathing in these lasers, so that the pulse shape is Gaussian rather than hyperbolic secant [16].

Stretched-pulse fiber lasers, as well as the recently developed dissipative soliton lasers [19] (including all-normal dispersion lasers [20], self-similar pulse lasers [21], and soliton-similariton fiber lasers [22]), have been successfully used to generate sub-100-fs pulses with broad optical bandwidths, typically tens of nanometers, which is close to or even broader than the gain bandwidth of the EDF amplifier. The large spectral breathing in such lasers, however, demands intracavity pulse energies from several nanojoules to tens of nanojoules [20–23], which is much higher than the tens of picojoules pulse energies that are needed in soliton fiber lasers [8–10]. Nanojoule-level pulse energies are useful in many practical applications, and at the megahertz-order pulse repetition rates typical of mode-locked fiber lasers, the average power is only tens to hundreds of milliwatts. When, however, the pulse repetition rate is increased to gigahertz by harmonic mode locking, the average signal power in the laser cavity must rise to several watts if stretched-pulse or dissipative soliton formation is to be maintained. The demand for such high powers from the laser oscillator generally involves complicated pump configurations and produces thermal instabilities, challenging the practical implementation of these lasers. As a result, all-fiber laser configurations that simultaneously offer gigahertz repetition rates and sub-100-fs pulse durations are rarely found in the literature [24,25].

In this paper, we report an Er-doped all-fiber laser in which the intracavity pulses evolve in a unique "stretched-soliton" manner, generating ultrashort (sub-100-fs) soliton-like pulses with intracavity pulse energies of only tens of picojoules. Strong dispersion management in the laser cavity is achieved by inserting dispersion-compensating fibers (DCFs) with high normal dispersion, resulting in an intracavity temporal breathing ratio of ~70. Together with the low energy of the laser pulses, this dramatically reduces the effect of the Kerr nonlinearity, minimizing nonlinear spectral reshaping within the laser cavity. The basic balance underlying this "stretched-soliton" formation, similar to that in a soliton fiber laser, is between the weak effective Kerr nonlinearity and the small residual anomalous dispersion, yielding broadband soliton-like pulses. In order to ensure the self-consistency of the laser pulses, the spectral filtering introduced by the wavelength-dependent gain of the EDF amplifier is compensated by a wavelength-dependent attenuator (WDA), realized through the combination of DCF birefringence and an in-line polarizer. This unique stretched-soliton configuration permits the generation of broadband soliton-like pulses at intracavity pulse energies that are ~10 times lower, with temporal breathing ratios ~10 times higher, than in conventional stretched-pulse or dissipative soliton fiber lasers [15,19]. These characteristics make the stretched-soliton laser suitable for generating high-repetition-rate broadband (ultrashort) pulse trains. High-harmonic mode locking (HHML) via intense optoacoustic interactions in a short length of solid-core photonic crystal fiber (PCF) [26–28] results in the generation of a stable 1.873 GHz pulse train with hyperbolic-secant sub-100-fs pulses in an all-fiber laser configuration without cladding pumping.

2. EXPERIMENTAL SETUP

A schematic of the fiber ring laser used in the experiments is shown in Fig. 1. The laser gain medium was a 1.05 m length of EDF with 110 dB/m peak absorption at 1530 nm, pumped at 976 nm by two laser diodes (LD–1 and LD–2) with a combined power of 1.5 W. The 2-m-long PCF inserted in the laser cavity had a core diameter of 1.95 μm [see the scanning electron micrograph (SEM) in Fig. 1], with an R_{01} acoustic core resonance at 1.882 GHz [28] and high anomalous dispersion of −157 ps^2/km at 1550 nm. In the PCF–SMF splicing, a short length of ultrahigh-NA fiber was used as a transition fiber, leading to ~1.7 dB insertion loss for the PCF. The intrinsic PCF loss is ~0.05 dB/m. Two lengths of DCF (3.0 and 0.8 m) with identical dispersion (+121 ps^2/km at 1550 nm) were spliced into the laser cavity, resulting in a total cavity dispersion of −0.008 ± 0.003 ps^2.

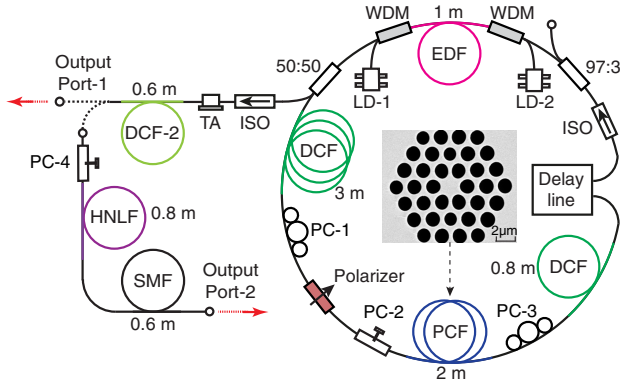

Fig. 1. Experimental setup (see text for details). The SEM shows the PCF microstructure. WDM, wavelength-division multiplexer.

Two polarization controllers (PC-1 and PC-3) and a fiber-coupled polarizer were used to configure a fast saturable absorber based on nonlinear polarization rotation, enabling the self-starting of mode locking [29]. PC-2, before the PCF, was used to adjust the polarization state of light launched into the PCF. A delay line was used to adjust the cavity length, an optical isolator (ISO) ensured unidirectional operation, and a 50:50 coupler was used to extract light from the laser. All components in the laser cavity, with the exceptions of the EDF, DCF, and PCF, were made from conventional SMF with an anomalous dispersion of −22.5 ps^2/km. The total cavity loss was ~13 dB, and the cavity length was 17.2 m, corresponding to a cavity mode spacing of 12.1 MHz.

3. RESULTS

A. HHML Pulse Train

The laser had a CW-lasing threshold of ~100 mW, and stable HHML could be achieved at pump powers greater than 1 W by carefully adjusting all three PCs in the laser cavity [27,28]. When the pump power was further increased to its maximum value of 1.5 W, stable HHML at 1.873 GHz could be maintained, provided that the PCs were properly adjusted. In this process of increasing the pump, we observed that the laser output power increased by ~20%. At a pump power of 1.5 W the laser output power from the 50:50 coupler was 158 mW, corresponding to a maximum intracavity average signal power of ~340 mW. The output pulse train was recorded using a 33 GHz photodetector and a 16 GHz oscilloscope. A typical result is shown in Fig. 2(a), monitored over 300 h using an oscilloscope operating in

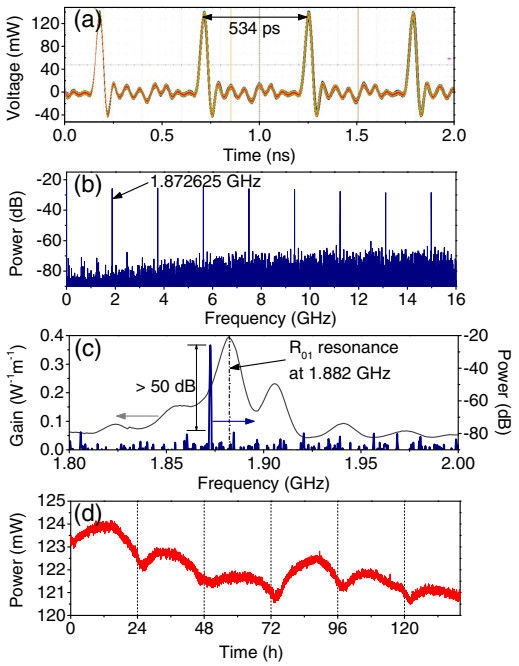

Fig. 2. (a) Output pulse train recorded over 300 h by an oscilloscope in persistence mode, (b) RF spectrum of the pulse train, (c) zoomed-in plot of the RF spectrum (blue curve) in the vicinity of 1.873 GHz. The optoacoustic gain band of the R_{01} acoustic resonance in the PCF core is plotted as the gray curve [27]. (d) Long-term recording of the laser output power.

infinite persistence mode. The RF spectrum of the pulse train, measured using a 26.5 GHz electrical spectrum analyzer, is shown in Fig. 2(b). The first harmonic peak at 1.873 GHz corresponds to the 155th harmonic of the cavity mode spacing, located at the lower-frequency side of the acoustic resonance [26,27]. The pulse repetition rate could be tuned within a range of ~7 MHz (from 1.869 to 1.876 GHz) by adjusting the intracavity delay line, while the laser was stably mode locked with invariant harmonic order [28]. The supermode noise suppression ratio was measured to be over 50 dB, as shown in Figs. 2(b) and 2(c). The short-term pulse amplitude noise was measured to be less than 0.1% (from 20 Hz to 1 MHz), and the pulse timing jitter was less than 50 fs (200 Hz to 1 MHz) [28].

HHML could be stably maintained over a few weeks without external stabilization or re-adjustment. We also observed that the average output power varied by ~3% with a period of 24 h, as shown in Fig. 2(d), which we attribute to the daily temperature cycle in the laboratory. After turning off and restarting the laser, the pulse train at 1.873 GHz could be easily reproduced by adjusting the PCs. At pump powers higher than 1 W the laser always reached a harmonically mode-locked state with a pulse repetition rate lying within the optoacoustic gain band of the PCF, as shown in Fig. 2(c). The acoustic resonant frequency of the PCF is mainly determined by its core diameter and air-filling fraction [30], and can vary from several hundreds of megahertz to a few gigahertz. When HHML is operating, the pulse repetition rate could be slightly tuned over a frequency range of several megahertz by adjusting the tunable delay line, so long as locking to the acoustic resonance in the PCF core was maintained [27,28].

B. Laser Pulse Duration and Optical Spectrum

The optical spectrum of the laser pulses measured at the 50:50 output coupler is shown by the red curve in Fig. 3(a), with a 3 dB bandwidth of 20.9 nm. The spectrum has a smooth profile without Kelly sidebands or noisy spikes, indicating a low background noise level. The spectral density shown here as well as in all the other optical spectra in this paper are relative values. Hence, they only illustrate spectral profiles and relative energy levels

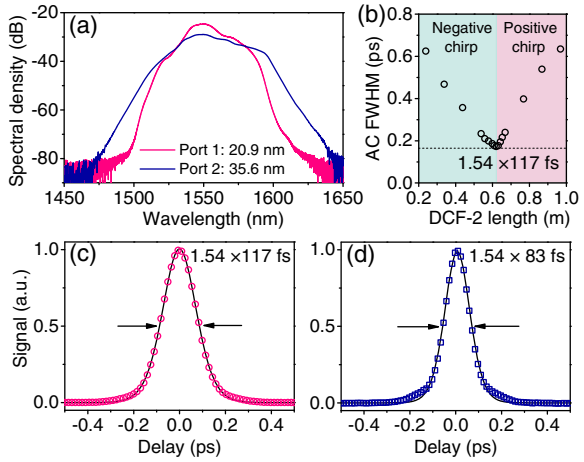

Fig. 3. (a) Optical spectrum measured at output port 1 and port 2, (b) chirp compensation of laser pulses for different DCF-2 lengths (via the cutback method). The widths of the pulse autocorrelation (AC) traces are plotted. (c), (d) Autocorrelation traces at port 1 and port 2 with fitting curves, assuming a sech^2 pulse shape.

at different positions. As shown in Fig. 1, the output pulse train was delivered through an optical ISO and a tunable attenuator (TA) so as to avoid backscattered light from the diagnostic setup entering the laser cavity. After the attenuator, a short length of DCF (DCF-2) with dispersion +45 ps^2/km at 1550 nm was used to compensate the residual pulse chirp. A cutback method, as shown in Fig. 3(b), was used to obtain the shortest de-chirped pulse duration. With a 0.62-m-long DCF-2 fiber, the smallest measured full width at half-maximum (FWHM) pulse duration was ~117 fs (180 fs autocorrelation width), estimated by fitting the data to a hyperbolic-secant function, as shown in Fig. 3(c). The time–bandwidth product (TBP) was calculated to be ~0.31, in good agreement with that of a transform-limited hyperbolic-secant pulse.

C. Extra-Cavity Spectral Broadening and Pulse Compression

The average power at output port 1 was measured to be ~112 mW, corresponding to a pulse energy of ~60 pJ. Considering a pulse duration of 117 fs, the pulse peak power at this port was estimated to be over 500 W. In the experiments, these transform-limited pulses were spectrally broadened by launching into a 0.8 m length of highly nonlinear fiber (HNLF), as shown in Fig. 1. The HNLF had a Kerr nonlinearity coefficient of 10.9 $W^{-1}\,km^{-1}$ and a normal dispersion of 16.5 ps^2/km. A polarization controller (PC-4) was inserted before the HNLF to adjust the polarization state of the pulses launched into the HNLF. The spectrum of the broadened pulses is plotted in Fig. 3(a) (blue curve), showing a 3 dB bandwidth of 35.6 nm. The resulting pulses were then de-chirped in a 0.6 m length of SMF, leading to a pulse duration of ~83 fs, as shown in Fig. 3(d), and the TBP was calculated to be ~0.37. The larger TBP and the deviation of the pulse profile from a hyperbolic-secant shape, as shown in Fig. 3(d), mainly results from the highly nonlinear pulse propagation [16]. The average output power at port 2 was measured to be ~76 mW, corresponding to a pulse energy of ~41 pJ.

4. PRINCIPLE OF OPERATION

A. Numerical Simulations and Experimental Validation

To understand stretched-soliton formation in the strongly dispersion-managed fiber laser cavity, the laser was numerically simulated using the symmetrized split-step Fourier method [12]. In the simulations, only one laser pulse was studied for simplicity, the assumption being that all 155 pulses evolve in a similar manner in the fiber cavity—this is certainly true in the steady state. As shown in Fig. 4(a), the laser loop used in the simulations contains eight fiber sections with alternating normal and anomalous dispersion; two lumped optical components were also introduced to model the in-line polarizer and the 50:50 output coupler. The dispersion map of the fiber laser is shown in Fig. 4(a), and the Kerr nonlinearity coefficients of the SMF, DCF, and PCF used in the simulations were 1.1, 2.86, and 28.6 $W^{-1}\,km^{-1}$. A WDA was included in the simulations, located at the in-line polarizer, as shown in Fig. 4(a), with a central wavelength of 1550 nm, a bandwidth of 40 nm, and an attenuation peak of ~6 dB. A detailed discussion of this WDA and the balance between spectral filtering effects in the laser cavity is available in the next section.

In the simulations, an initial pulse of duration ~100 ps was launched into the laser loop, and its evolution was followed over

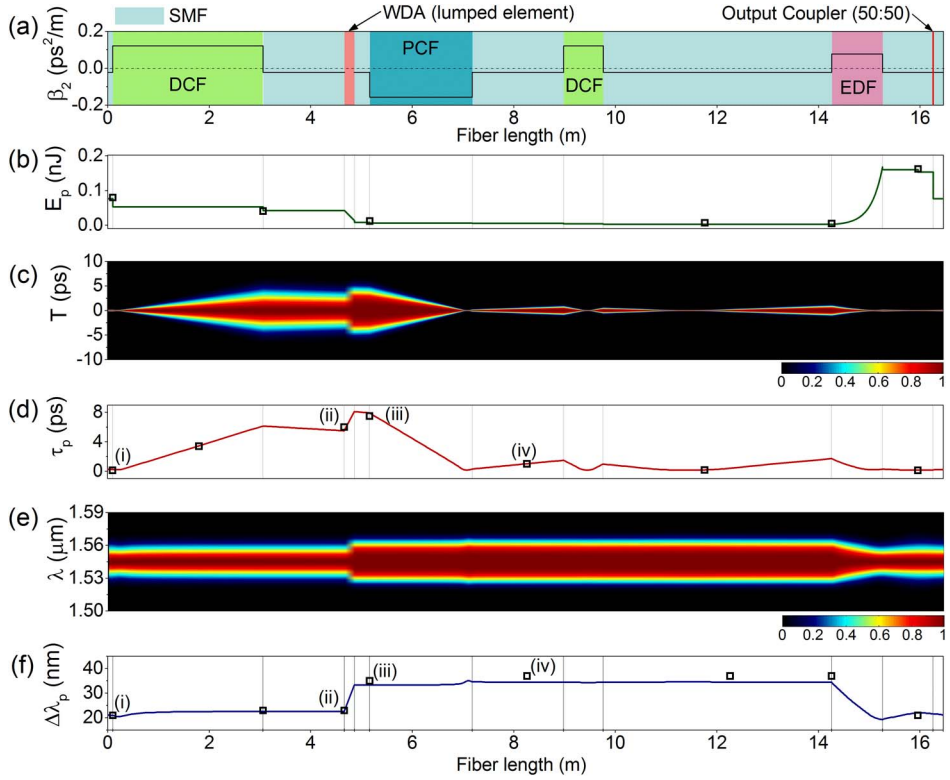

Fig. 4. (a) Laser loop and dispersion map used in the simulations; (b) pulse energy evolution around the laser cavity; (c), (d) evolution of pulse shape and pulse FWHM duration; (e), (f) evolution of pulse spectrum and 3 dB bandwidth.

several thousand round trips until the steady state was reached. In this process, a gain saturation element was used to fix the pulse energy at the experimental value, while a fast saturable absorber was included to accelerate self-starting of mode locking. In the steady state, neither gain saturation nor fast saturable absorber effects contribute significantly to pulse shaping. These two effects function rather as weak "noise eaters," stabilizing the steady state (when they are removed from the simulations, the pulses destabilize after several hundred round trips).

The evolution of the pulse energy is shown in Fig. 4(b). The total cavity loss is ~19 dB (~13 dB total component loss together with an extra ~6 dB from the WDA). The intracavity temporal and spectral evolution of the pulses in the steady state are shown as color maps in Figs. 4(c) and 4(e). Both the temporal and spectral pulse profiles are normalized at each position in the laser loop. The variations in FWHM pulse duration and spectral width in the laser cavity, estimated using the simulated data, are plotted as solid curves in Figs. 4(d) and 4(f). As shown in Fig. 4(d), a temporal breathing ratio of ~70 (from ~110 fs to ~8 ps) is observed, which is some 10 times greater than that seen in conventional stretched-pulse and dissipative soliton lasers [15,22]. On the other hand, the spectral breathing ratio is ~1.7 [from ~20 to ~35 nm, as shown in Fig. 4(f)], and major spectral variations occur only at two localized positions in the laser loop, leaving the spectral bandwidth almost unchanged at other positions, as seen in Figs. 4(e) and 4(f). The WDA is designed to counteract bandwidth narrowing due to wavelength-dependent gain in the EDF amplifier.

In order to experimentally monitor pulse evolution between the 50:50 coupler and the 97:3 coupler (see Fig. 1), we built an external replica of that part of the laser loop, including SMFs, DCFs, PCF, polarizer, and three PCs. Under stable HHML, pulses from the output port of the 50:50 coupler were launched into this replica, permitting experimental retrieval of the pulse evolution within the laser cavity. The measured pulse durations and spectral widths at different positions are shown as square dots in Figs. 4(b), 4(d), and 4(f), and agree well with the simulations. Autocorrelation traces and optical spectra measured at four different positions are shown in Fig. 5, indicating the temporal breathing and spectral variations in the cavity.

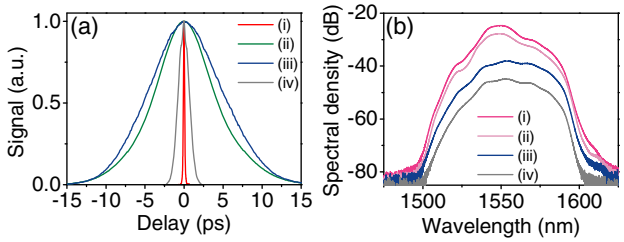

Fig. 5. (a) Pulse autocorrelation traces and (b) optical spectra measured at different positions in the laser cavity.

B. Wavelength-Dependent Attenuator

Key factors enabling the generation of broadband hyperbolic-secant pulses are the relatively low energy and large temporal breathing of the pulses, which nearly eliminate nonlinear spectral reshaping. As the bandwidth broadens, the gain filtering effect in the EDF increases and must be balanced on each cavity round

trip if self-consistent pulse propagation is to be obtained. In conventional stretched-pulse fiber lasers, this gain filtering effect is balanced by nonlinear spectral broadening, which is a major reason why high pulse energies (nanojoule-order) are needed in such lasers [19]: high pulse energies imply a strong Kerr effect, which, operating in concert with the pulse chirp, results in strong spectral broadening in a length of normal-dispersion fiber.

In the stretched-soliton fiber laser, on the other hand, the wavelength-dependent gain peak in the EDF is counterbalanced by a WDA, which is formed by the combination of the 3-m-long birefringent ($B = \sim 1 \times 10^{-5}$) DCF and a polarizer. These parameters yielded a free spectral range of 80 nm between WDA transmission peaks, and the system was adjusted using PC-1 and PC-3 so that a transmission minimum (–6 dB deep) coincided with the peak gain of the EDF amplifier [31].

Effective "spectral broadening" in the WDA was verified experimentally by making measurements before and after the in-line polarizer. As shown in Fig. 6(a), the bandwidth of pulses broadened from 22.6 nm (blue curve) to 35.0 nm (gray curve), while the peak spectral density was reduced by ~6 dB. WDA-induced spectral broadening was also observed in the simulations, as shown in Fig. 6(b). The measured (solid curve) and simulated (dashed curve) WDA profiles are plotted in Fig. 6(c). Both have an ~40 nm optical bandwidth and ~6 dB modulation depth at the filter center. The spectral narrowing effect in the EDF was also measured by comparing the pulse spectrum before and after the EDF, using the 97:3 and 50:50 output couplers, as shown in Fig. 1. The profile of the gain filter shown in Fig. 6(d) closely resembles the profile of the measured WDA shown in Fig. 6(c), but with the opposite sign.

The balance between wavelength-dependent gain and attenuation is similar to the concept of gain flattening in optical amplifiers [32,33], and has been recently used in semiconductor [34] and bulk-material mode-locked lasers [35,36]. In the stretched-soliton laser, while the balance between wavelength-dependent gain and attenuation permits spectral-domain self-consistency in a low-nonlinearity cavity, strong dispersion management broadens the pulses dramatically in the temporal domain, permitting the generation of broadband stretched solitons with low pulse energy.

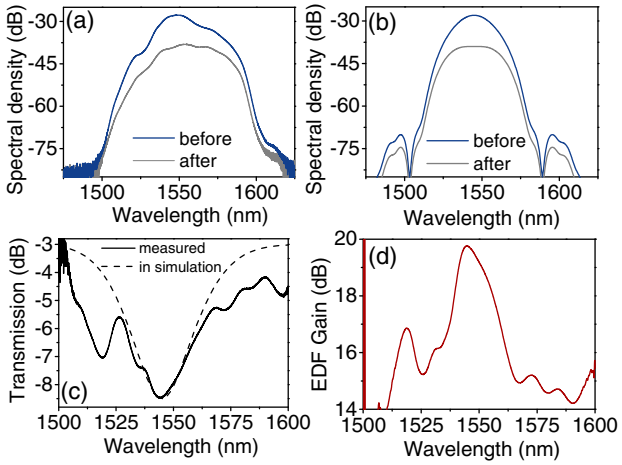

Fig. 6. (a) Measured and (b) simulated pulse spectra before and after the intracavity polarizer, (c) transmission profiles of the intracavity WDA, calculated using experimental data (solid curve) and those used in the simulations (dashed curve), (d) measured gain spectrum in the EDF.

C. Soliton-Like Balance

Even though strong dispersion management leads to large temporal breathing in the stretched-soliton laser, the underlying balance is similar to that seen in soliton fiber lasers: nonlinear effects and weak residual anomalous dispersion produces hyperbolic-secant pulses, rather than the Gaussian pulses typical of conventional stretched-pulse fiber lasers [37]. Due to the low pulse energy and large temporal breathing ratio, energy redistribution between different spectral components of laser pulses is negligibly small, so that this soliton-like balance is easier to understand in the spectral domain.

In a group velocity frame of the laser pulse, the spectral envelope of the pulse $\tilde{A}(\omega, z)$ is the Fourier transform of the pulse electrical field envelope $A(t, z)$. Over a single cavity round trip, the accumulated phase shift for each spectral component due to cavity dispersion is given by

$$\tilde{\phi}_{\mathrm{GVD,total}}(\omega) = \frac{1}{2}\omega^2 \int_0^L \beta_2(z)\mathrm{d}z, \tag{1}$$

where L is the total cavity length and $\beta_2(z)$ describes the cavity dispersion map.

When considering only the Kerr nonlinearity, the pulse electrical field envelope after a propagation step dz becomes

$$A_{\mathrm{NL}}(t, z + dz) = A(t, z)\exp(i\gamma(z)|A(t, z)|^2)\mathrm{d}z, \tag{2}$$

where $\gamma(z)$ describes the Kerr nonlinearity distribution in the laser cavity. The nonlinear phase shift of the laser pulse as function of frequency can be expressed as

$$d\tilde{\phi}_{\mathrm{NL}}(\omega, z) = \arg\left[\frac{\tilde{A}_{\mathrm{NL}}(\omega, z + dz)}{\tilde{A}(\omega, z)}\right], \tag{3}$$

where $\tilde{A}_{\mathrm{NL}}(\omega, z + dz)$ is the Fourier transform of $A_{\mathrm{NL}}(t, z + dz)$. The accumulated nonlinear phase shift over a single cavity round trip can then be calculated using

$$\tilde{\phi}_{\mathrm{NL,total}}(\omega) = \int_0^L \mathrm{d}\tilde{\phi}_{\mathrm{NL}}(z, \omega). \tag{4}$$

Using Eqs. (1)–(4), we calculated the accumulated phase shifts of the laser pulse due to cavity dispersion and nonlinearity separately using the simulation results. The results are plotted as solid curves in Fig. 7, while the pulse spectrum at the laser output coupler is the dashed black curve. The sum of these nonlinearity-induced and dispersion-induced phase shifts is almost zero close to the spectral center, indicating almost complete cancellation.

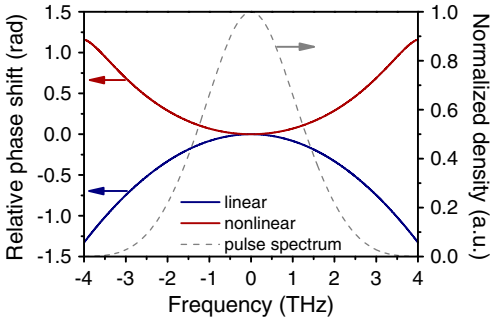

Fig. 7. Calculated phase shifts of laser pulses over a single cavity round trip due to cavity dispersion (blue solid curve) and nonlinearity (red solid curve). The stimulated spectrum of laser pulses is also plotted as a gray dashed curve.

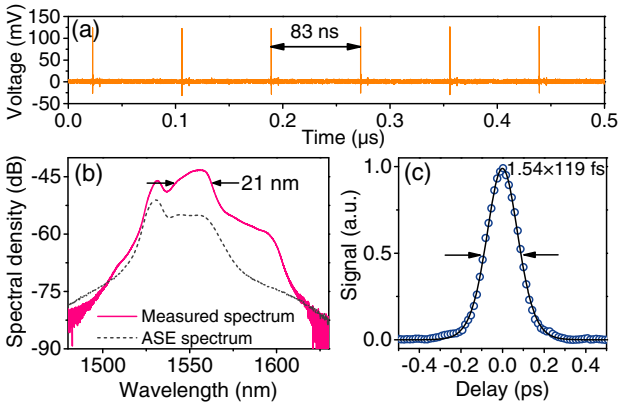

Fig. 8. (a) Fundamentally mode-locked pulse train at a 12.1 MHz repetition rate, obtained at a low pump power, (b) optical spectrum of the pulse train (red solid curve), showing considerable ASE noise. The measured ASE noise spectrum is also plotted as the gray dashed curve. (c) Measured autocorrelation trace of the 12.1 MHz pulse train with a fitting curve assuming a sech^2-shaped pulse.

Phase cancellation implies that different spectral components of laser pulses have the same overall group delay over a single cavity round trip, demonstrating self-consistent pulse evolution in the laser cavity. Small discrepancies observed at the edge frequencies are most probably due to the saturable absorber and higher-order dispersion in the laser cavity. As shown in Fig. 7, the accumulated nonlinear phase shift over one cavity round trip is well below π, indicating a low-nonlinearity laser cavity.

D. Fundamental Mode-Locked State

The stretched-soliton formation mechanism is independent of the number of pulses in the fiber laser cavity, and could therefore also be used to generate megahertz-rate ultrashort pulses at low laser power levels. To demonstrate this, we gradually decreased the pump power while the laser was oscillating and observed that optoacoustic HHML collapsed at a pump power less than 1 W. Further decreasing the pump power gradually reduced the number of pulses circulating in the laser cavity. As the pump power approached the lasing threshold, the fundamental mode-locked state, corresponding to a single pulse circulating in the laser cavity, was observed, with a pulse repetition rate of 12.1 MHz, as shown in Fig. 8(a). Despite considerable pulse drop-out as the pump power is reduced, both the spectral width and temporal duration of the pulses remained almost invariant. The optical spectrum and autocorrelation trace of the 12.1 MHz pulse train were measured, and the results are in Figs. 8(b) and 8(c), showing a spectral width of ~21 nm and a temporal duration of 119 fs. Because the laser was oscillating just above its threshold, there is strong amplified spontaneous emission (ASE) noise in the laser spectrum, as seen in Fig. 8(b). The average signal power in the laser cavity was measured to be only ~1 mW, corresponding to a pulse energy of tens of picojoules, similar to that of the pulses in the laser cavity in the HHML state.

5. DISCUSSION AND CONCLUSIONS

The formation of broadband hyperbolic-secant pulses in the stretched-soliton laser is made possible by its unique configuration: (1) the gain filtering effect in the EDF amplifier is balanced by the wavelength-dependent attenuation in the WDA; (2) the large temporal breathing of laser pulses, combined with the low pulse energy, nearly eliminates nonlinear spectral reshaping in the laser cavity. Moreover, the use of three periods of alternating normal and anomalous dispersion is necessary for stable harmonic mode locking because it forces the duration of the intracavity pulses to strongly oscillate several times over one cavity round trip. Correspondingly, the phase-matched frequencies of four-wave mixing are far from the pulse central frequency [38]. As shown in Fig. 3(a), the result is a smooth pulse spectrum without Kelly sidebands or noisy spikes. This dispersive-wave-free characteristic largely suppresses unwanted pulse-to-pulse interactions [14,39], permitting stable optoacoustic mode locking with relatively weak anomalous dispersion [26–28]. Using 2-m-long solid-core PCF as a HHML element in this stretched-soliton fiber laser, stable soliton-like pulse trains are produced at 1.5 W pump power, with over 20 nm optical bandwidth, sub-100-fs pulse duration, and 1.873 GHz pulse repetition rate.

Funding. Max Planck Society (MPG); Alexander von Humboldt Foundation.

Acknowledgment. The work of C. R. Menyuk was carried out in part while he was an Alexander von Humboldt senior fellow visiting the Max Planck Institute for the Science of Light.

REFERENCES

1. M. E. Fermann and I. Hartl, "Ultrafast fibre lasers," Nat. Photonics **7**, 868–874 (2013).
2. C. Jauregui, J. Limpert, and A. Tunnermann, "High-power fibre lasers," Nat. Photonics **7**, 861–867 (2013).
3. S. T. Cundiff and A. M. Weiner, "Optical arbitrary waveform generation," Nat. Photonics **4**, 760–766 (2010).
4. T. Udem, R. Holzwarth, and T. W. Hansch, "Optical frequency metrology," Nature **416**, 233–237 (2002).
5. C. Kerse, H. Kalaycıoğlu, P. Elahi, B. Çetin, D. K. Kesim, Ö. Akçaalan, S. Yavaş, M. D. Aşık, B. Öktem, H. Hoogland, R. Holzwarth, and F. Ö. Ilday, "Ablation-cooled material removal with ultrafast bursts of pulses," Nature **537**, 84–88 (2016).
6. I. N. Duling III, "All-fiber ring soliton laser mode locked with a nonlinear mirror," Opt. Lett. **16**, 539–541 (1991).
7. I. N. Duling III, "Subpicosecond all-fibre erbium laser," Electron. Lett. **27**, 544–545 (1991).
8. K. Tamura, H. A. Haus, and E. P. Ippen, "Self-starting additive pulse mode-locked erbium fibre ring laser," Electron. Lett. **28**, 2226–2228 (1992).
9. M. E. Fermann, "Ultrashort-pulse sources based on single-mode rare-earth-doped fibers," Appl. Phys. B **58**, 197–209 (1994).
10. D. J. Jones, H. A. Haus, and E. P. Ippen, "Subpicosecond solitons in an actively mode-locked fiber laser," Opt. Lett. **21**, 1818–1820 (1996).
11. L. E. Nelson, D. J. Jones, K. Tamura, H. A. Haus, and E. P. Ippen, "Ultrashort-pulse fiber ring lasers," Appl. Phys. B **65**, 277–294 (1997).
12. G. P. Agrawal, *Nonlinear Fiber Optics* (Academic, 2007).
13. D. U. Noske, N. Pandit, and J. R. Taylor, "Source of spectral and temporal instability in soliton fiber lasers," Opt. Lett. **17**, 1515–1517 (1992).
14. N. Pandit and J. R. Taylor, "Characterstic instability of fibre loop soliton lasers," Electron. Lett. **28**, 455–457 (1992).
15. K. Tamura, E. P. Ippen, H. A. Haus, and L. E. Nelson, "77-fs pulse generation from a stretched-pulse mode-locked all-fiber ring laser," Opt. Lett. **18**, 1080–1082 (1993).
16. K. Tamura, L. E. Nelson, H. A. Haus, and E. P. Ippen, "Soliton versus nonsoliton operation of fiber ring lasers," Appl. Phys. Lett. **64**, 149–151 (1994).
17. H. A. Haus, K. Tamura, L. E. Nelson, and E. P. Ippen, "Stretched-pulse additive pulse mode-locking in fiber ring lasers: theory and experiment," IEEE J. Quantum Electron. **31**, 591–598 (1995).
18. K. Tamura, E. P. Ippen, and H. A. Haus, "Pulse dynamics in stretched-pulse fiber lasers," Appl. Phys. Lett. **67**, 158–160 (1995).

19. P. Grelu and N. Akhmediev, "Dissipative solitons for mode-locked lasers," Nat. Photonics **6**, 84–92 (2012).
20. F. W. Wise, A. Chong, and W. H. Renninger, "High-energy femtosecond fiber lasers based on pulse propagation at normal dispersion," Laser Photon. Rev. **2**, 58–73 (2008).
21. F. Ö. Ilday, J. R. Buckley, W. G. Clark, and F. W. Wise, "Self-similar evolution of parabolic pulses in a laser," Phys. Rev. Lett. **92**, 213902 (2004).
22. B. Öktem, C. Ulgudur, and F. Ö. Ilday, "Soliton-similariton fibre laser," Nat. Photonics **4**, 307–311 (2010).
23. M. E. Fermann, M. J. Andrejco, Y. Silberberg, and A. M. Weiner, "Generation of pulses shorter than 200 fs from a passively mode-locked Er fiber laser," Opt. Lett. **18**, 48–50 (1993).
24. C. Li, Y. Ma, X. Gao, F. Niu, T. Jiang, A. Wang, and Z. Zhang, "1 GHz repetition rate femtosecond Yb:fiber laser for direct generation of carrier-envelope offset frequency," Appl. Opt. **54**, 8350–8353 (2015).
25. C. X. Yu, H. A. Haus, E. P. Ippen, W. S. Wong, and A. Sysoliatin, "Gigahertz-repetition-rate mode-locked fiber laser for continuum generation," Opt. Lett. **25**, 1418–1420 (2000).
26. M. Pang, W. He, X. Jiang, and P. St.J. Russell, "All-optical bit storage in a fibre laser by optomechanically bound states of solitons," Nat. Photonics **10**, 454–458 (2016).
27. M. Pang, X. Jiang, W. He, G. K. L. Wong, G. Onishchukov, N. Y. Joly, G. Ahmed, C. R. Menyuk, and P. St.J. Russell, "Stable subpicosecond soliton fiber laser passively mode-locked by gigahertz acoustic resonance in photonic crystal fiber core," Optica **2**, 339–342 (2015).
28. W. He, M. Pang, and P. St.J. Russell, "Wideband-tunable soliton fiber laser mode-locked at 1.88 GHz by optoacoustic interactions in solid-core PCF," Opt. Express **23**, 24945–24954 (2015).
29. K. Tamura, J. Jacobson, E. P. Ippen, H. A. Haus, and J. G. Fujimoto, "Unidirectional ring resonators for self-starting passively mode-locked lasers," Opt. Lett. **18**, 220–222 (1993).
30. M. S. Kang, A. Nazarkin, A. Brenn, and P. St.J. Russell, "Tightly trapped acoustic phonons in photonic crystal fibres as highly nonlinear artificial Raman oscillators," Nat. Phys. **5**, 276–280 (2009).
31. K. Özgören and F. Ö. Ilday, "All-fiber all-normal dispersion laser with a fiber-based Lyot filter," Opt. Lett. **35**, 1296–1298 (2010).
32. C. P. J. Barty, G. Korn, F. Raksi, A. C. Tien, K. R. Wilson, V. V. Yakovlev, C. Rose-Petruck, J. Squier, and K. Yamakawa, "Regenerative pulse shaping and amplification of ultrabroadband optical pulses," Opt. Lett. **21**, 219–221 (1996).
33. J. Seres, A. Müller, E. Seres, K. O'Keeffe, M. Lenner, R. F. Herzog, D. Kaplan, C. Spielmann, and F. Krausz, "Sub-10-fs, terawatt-scale Ti:sapphire laser system," Opt. Lett. **28**, 1832–1834 (2003).
34. J. S. Parker, R. S. Guzzon, E. J. Norberg, A. Bhardwaj, P. R. A. Binetti, and L. A. Coldren, "Theory and design of THz intracavity gain-flattened filters for monolithically integrated mode-locked lasers," IEEE J. Quantum Electron. **48**, 114–122 (2012).
35. L.-J. Chen, M. Y. Sander, and F. X. Kärtner, "Kerr-lens mode locking with minimum nonlinearity using gain-matched output couplers," Opt. Lett. **35**, 2916–2918 (2010).
36. C. Cihan, E. Beyatli, F. Canbaz, L. J. Chen, B. Sumpf, G. Erbert, A. Leitenstorfer, F. X. Kärtner, A. Sennaroglu, and U. Demirbas, "Gain-matched output couplers for efficient Kerr-lens mode-locking of low-cost and high-peak power Cr:LiSAF lasers," IEEE J. Sel. Top. Quantum Electron. **21**, 94–105 (2015).
37. S. K. Turitsyn, B. G. Bale, and M. P. Fedoruk, "Dispersion-managed solitons in fibre systems and lasers," Phys. Rep. **521**, 135–203 (2012).
38. M. L. Dennis and I. N. Duling III, "Intracavity dispersion measurement in modelocked fibre laser," Electron. Lett. **29**, 409–411 (1993).
39. R. P. Davey, N. Langford, and A. I. Ferguson, "Interacting solutions in erbium fibre laser," Electron. Lett. **27**, 1257–1259 (1991).